

NDOT Research Report

Report No: RDT02-030

**A PRELIMINARY STUDY
OF SHAKE TABLE
RESPONSE OF A TWO-
COLUMN BRIDGE BENT
ON FLEXIBLE FOOTINGS**

November 2002

Prepared by Research Division
Nevada Department of Transportation
1263 South Stewart Street
Carson City, Nevada 89712



TECHNICAL REPORT DOCUMENTATION PAGE

1. Report No. RDT-02-030		2. Government Accession No.	3. Recipients Catalog No.
4. Title and Subtitle A Preliminary Study of Shake Table Response of A Two-Column Bridge Bent on Flexible Footings		5. Report Date June 2002	
		6. Performing Organization Code	
7. Author(s) M. Saiidi, B. Gopalakrishnan, E Reinhardt, and R. Siddharthan		8. Performing Organization Report No. CCEER-02-03	
9. Performing Organization Name and Address Department of Civil Engineering Earthquake Research University of Nevada, Reno Reno, Nevada 89557		10. Contract Title Seismic Performance of Bridge Bents with Unretrofitted Footings	
		11. Contract or Grant No. P442-99-803	
12. Sponsoring Agency Name and Address Nevada Department of Transportation Research Division 1263 S. Stewart Street Carson City, NV 89712		13. Type or Report and Period Covered 06-01-1999 to 06-30-2001	
		14. Sponsoring Agency Code	
15. Supplementary Notes			
16. Abstract <p>The main objective of this study was to determine the effect of footing flexibility on the dynamic response of large-scale two-column bridge bents subjected to earthquake loads simulated on a shake table. A quarter-scale bent with two square columns supported on spread footings was the subject of the study. The beam and the columns incorporated several innovative features with respect to the plastic hinge location and application of carbon fiber reinforced plastics. However, these issues were not the focus of the study presented in this report. Of particular relevance to this study was simulation of translational and rocking flexibility of soil through elastomeric bearing pads that were placed underneath and on the sides of the footings. Three footing configurations were studied. One was with substandard footings resting on flexible supports, another with retrofitted footings resting on flexible supports, and the third with footings that were fixed to the shake table. The testing of cases with flexible footings was essentially in the linear range so that the frame above the footings could be saved for the fixed base study, in which loading continued until failure. Results showed a substantial reduction in the steel bar strains near the base of the columns as a result of footing flexibility. Reduction in strains elsewhere in the bent and the footings was also significant, but to a lesser extent. The results strongly suggest that retrofit requirements at column bases to address lap splices and low shear and confinement reinforcement may be reduced when the beneficial effects of soil flexibility is accounted for.</p>			
17. Key Words Bridges, columns, seismic performance, un-retrofitted footings, footing flexibility, earthquake loads, shake tables		18. Distribution Statement Unrestricted. This document is available through the National Technical Information Service, Springfield, VA 21161	
19. Security Classif. (of this report) Unclassified	20. Security Classif. (of this page) Unclassified	21. No. Of Pages 73	22. Price

Report No. CCEER 02-3

**A Preliminary Study of Shake Table
Response of A Two-Column Bridge
Bent on Flexible Footings**

**M. Saiidi, B. Gopalakrishnan,
E. Reinhardt, and R. Siddharthan**

Prepared for

**Nevada Department of Transportation
Structural Design Division
Carson City, Nevada**

Center for Civil Engineering Earthquake Research

University of Nevada, Reno

June 2002

ACKNOWLEDGEMENTS

The study presented in this report was funded mainly by a grant from the Nevada Department of Transportation (NDOT)/Federal Highway Administration (FHWA) to the University of Nevada, Reno (UNR). Additional funds were provided by the National Science Foundation Grant CMS-9800080. However, the opinions expressed in the report are those of the authors and do not necessarily reflect the views of NDOT, FHWA, or NSF.

The authors thank Mr. Bill Crawford, Chief Bridge Engineer at NDOT, and other staff at NDOT Bridge Division for their support and advice in the course of this project. Messrs. Patrick Laplace, Paul Lucas, Cole Mortensen, and Nathan Johnson are thanked for their contributions to testing and data processing in this project. Mitsubishi, Japan, donated the carbon fiber reinforced plastic fabrics through the Sumitomo Corporation of America. The generous assistance provided by Dr. Ali Ganjehlou of Sumitomo is much appreciated.

ABSTRACT

The main objective of this study was to determine the effect of footing flexibility on the dynamic response of large-scale two-column bridge bents subjected to earthquake loads simulated on a shake table. A quarter-scale bent with two square columns supported on spread footings was the subject of the study. The beam and the columns incorporated several innovative features with respect to the plastic hinge location and application of carbon fiber reinforced plastics. However, these issues were not the focus of the study presented in this report. Of particular relevance to this study was simulation of translational and rocking flexibility of soil through elastomeric bearing pads that were placed underneath and on the sides of the footings. Three footing configurations were studied. One was with substandard footings resting on flexible supports, another with retrofitted footings resting on flexible supports, and the third with footings that were fixed to the shake table. The testing of cases with flexible footings was essentially in the linear range so that the frame above the footings could be saved for the fixed base study, in which loading continued until failure. Results showed a substantial reduction in the steel bar strains near the base of the columns as a result of footing flexibility. Reduction in strains elsewhere in the bent and the footings was also significant, but to a lesser extent. The results strongly suggest that retrofit requirements at column bases to address lap splices and low shear and confinement reinforcement may be reduced when the beneficial effects of soil flexibility is accounted for.

TABLE OF CONTENTS

ACKNOWLEDGEMENTS	ii
ABSTRACT	iii
TABLE OF CONTENTS	iv
1. INTRODUCTION	
1.1 Introductory Remarks	1
1.2 Previous Work	2
1.3 Objectives and Scope	4
2. SPECIMENS AND TESTING PROGRAM	
2.1 Introductory Remarks	6
2.2 Design of the Test Structure	6
2.3 As-Built Footing Design	7
2.4 Retrofitted Footing Design	8
2.5 Construction of Test Specimen	10
2.6 Material Properties	11
2.7 Instrumentation	12
2.8 Program of Experimental Studies	13
2.8.1 Test Setup	13
2.8.2 Testing Program	15
3. MODELING SOIL FLEXIBILITY	
3.1 Introductory Remarks	18
3.2 Schmertmann's Method	18
3.2.1 Soil Vertical Stiffness	19
3.2.2 Soil Horizontal Stiffness	21
3.3 Equivalent Soil Stiffness for the Model	22
3.3.1 Average Normal and Shear Stresses on Footings	23
3.3.2 Evaluation of Soil Stiffness	23
3.4 Bearing Pads	24
3.4.1 Bearing Pad Stiffness	24
3.4.2 Bearing Pad Design	25
4. EFFECTS OF FOUNDATION FLEXIBILITY ON RESPONSE	
4.1 Introductory Remarks	27
4.2 Load-Displacement Response	27
4.3 Column Moments	28
4.4 Beam Moments	29
4.5 Joint Forces	30
4.6 Moment in Footings	30
4.7 Footing Displacements and Rotations	31
4.8 Contribution of Footing Displacement to Total Response	32
4.9 Design Implications	33

5. SUMMARY AND CONCLUSIONS

5.1	Summary.....	35
5.2	Conclusions.....	36

LIST OF TABLES

2.1	Measured Concrete Compressive Strength.....	41
2.2	Measured Tensile Strength of Steel Reinforcement.....	41
2.3	Testing Program for B2SA.....	42
2.4	Testing Program for B2SA.....	42
2.5	Testing Program for B2SF.....	43
3.1	Summary of Results for Soil Stiffness.....	44

LIST OF FIGURES

2.1	Elevation of B2SA.....	45
2.2	Cross Sections for the Beam and Columns.....	46
2.3	Steel Details and Gage Locations for the Left Column in B2SA.....	46
2.4	Steel Details and Gage Locations for the Right Column in B2SA.....	47
2.5	Plan View of the As-built footings.....	47
2.6	Plan View of the Retrofitted Footings.....	48
2.7	Elevation View of the Retrofitted Footings.....	48
2.8	Location of Threaded Rods for Curvature Measurement.....	49
2.9	Overall Test Set Up.....	49
3.1	Vertical Stress-settlement Relationship for the As-built Footing.....	50
3.2	Vertical Stress-settlement Relationship for the Prototype Retrofitted Footing.....	50
3.3	Horizontal Stress-displacement for Prototype As-built Footing.....	51
3.4	Horizontal Stress-displacement for Retrofitted Prototype Footing.....	51
3.5	Forces on Footing for Unit Downward Displacement.....	52
3.6	Forces on Footing for Unit Horizontal Displacement.....	52
3.7	Retrofitted Footing with Bearing Pads Highlighted for Clarity.....	53
4.1	Measured Top Horizontal Displacement vs Lateral Force.....	54
4.2	Strain Variation in Bottom Plastic Hinge in Left Column.....	54
4.3	Strain Variation in Top Hinge in Left Column.....	55
4.4	Strain Variation Near the Bottom Plastic Hinge in the Left Column.....	55
4.5	Strain Variation Near the Top Plastic Hinge in the Left Column.....	56
4.6	Strain Variation in Bottom Plastic Hinge in Right Column.....	56
4.7	Strain Variation in Top Plastic Hinge in Right Column.....	57
4.8	Strain Variation in Top Plastic Hinge in Right Column.....	57
4.9	Strain Variation in Top Beam Steel at the Left Column Face.....	58
4.10	Strain Variation in Top Beam Steel at the Right Column Face.....	58
4.11	Strain Variation in Bottom Beam Steel at the Right Column Face.....	59
4.12	Horizontal Strain Variation in the Left Joint.....	59

4.13	Vertical Strain Variation in the Right Joint.....	60
4.14	Horizontal Strain Variation in the Right Joint.....	60
4.15	Strain Variation in Left Side of Left Footing.....	61
4.16	Strain Variation in Right Side of Left Footing.....	61
4.17	Strain Variation in Left Side of Right Footing.....	62
4.18	Strain Variation in Right Side of Right Footing.....	62
4.19	Measured Average Footing Horizontal Displacement vs Lateral Force.....	63
4.20	Measured Footing Rotation vs Lateral Force.....	63
4.21	Comparison of Measured Footing Displacement and Top Displacement vs Lateral Force for B2SA.....	64
4.22	Comparison of Measured Footing Displacement and Top Displacement vs Lateral Force for B2SR.....	64
LIST OF CCEER PUBLICATIONS.....		65

Chapter 1

INTRODUCTION

1.1 Introductory Remarks

The 1989 Loma Prieta earthquake and the 1994 Northridge earthquake resulted in many bridges collapsing due to structural design that did not adequately consider seismic loading. Older bridge structures have historically been vulnerable to seismic loading, with numerous examples of damage occurring to both superstructure and substructure elements, and, in some cases, complete collapse. The watershed event in changing seismic design philosophies was the 1971 San Fernando earthquake. Bridges built under design criteria developed after 1971 have generally performed well in recent earthquakes. However, the vulnerability of older, pre-1971 bridges was clearly evident in the 1987 Whittier Narrows, the 1989 Loma Prieta, and the 1994 Northridge earthquakes. The Northridge earthquake resulted in the collapse of eleven overpasses on some of the busiest freeways in Los Angeles and the San Fernando Valley.

Past earthquakes and research on substandard bridges have shown clear patterns of deficiencies in pre-1971 structures. Typical deficiencies have included low confinement and shear reinforcement in structural members and connections, lap splice at column bases, insufficient footing plan view area, a lack of top steel in footings, etc. [1]. To correct these deficiencies, numerous analytical and experimental studies have been conducted on scaled models of bridge components and systems. To evaluate and address column deficiencies, all the past tests have been conducted on models that were fixed at the base [2]. The effect of soil flexibility was included only in a few studies that focused

on seismic performance of spread footings [3-5]. Assuming fixed base is conservative because it leads to largest demand on the columns, pier cap, and the joints. Seismic retrofit of bridge elements could be unnecessarily costly using the results of fixed-base column tests. It is generally known that soil-structure interaction can reduce the force demand in bridge components. However, no shake table studies of the soil-structure effect have been conducted in the past. The purpose of the preliminary study presented in this report was to examine and quantify the extent of reduction in seismic force demand in different parts of a two-column bridge pier tested under simulated earthquakes on a shake table.

1.2 Previous Work

A review of previous research was conducted to determine conclusions from past research and to evaluate their applicability to this study. Much research has been done on the subject of single-degree-of-freedom structures with rigid foundations. Flexible foundations with multi-degree-of-freedom structures are complicated systems, hence, very little research has been done on them. Individual footings beneath each column are also difficult to analyze and there is very little work done on this subject [6]. The soil-structure interaction effect on dynamic behavior of ordinary structures has not attracted much attention. Also, the experimental studies on dynamic behavior of such structures are rare in contrast to the large number of such studies on high-rise buildings and nuclear facilities. This may be due to the fact that the experimental evaluation of dynamic characteristics of short and squatty structures can be quite difficult [7]. It is believed that this is the first time a two-column bridge bent with as-built as well as retrofitted footings

resting on flexible foundations has been tested on a shake table. However, a number of studies of seismic assessment and retrofit of bridge footings, with footing and column sub-assemblages, have been done.

Acharya et al. [4,8] analyzed and tested 0.4 scale as-built and retrofitted reinforced concrete column-footing models under a constant axial load and cyclic lateral displacements simulating earthquakes. The focus was on spread footings and column footing connections. Retrofit measures included increasing footing dimensions to improve flexural capacity and reduce soil pressure under it, and providing a reinforced concrete overlay to minimize cracks. Additional measures were taken to enhance shear strength of plastic hinge in column and offset the effect of inadequate development of column reinforcement in the footing. The footings were supported on elastomeric bearing pads to simulate foundation horizontal and vertical stiffness.

McLean and Marsh [5] studied retrofitting measures for improving the seismic performance of the foundations of existing bridges. Retrofit measures for both pile-supported and spread footings were investigated. Tests were conducted on 1/3 scale footing and column sub-assemblages, supported on sand, which incorporated details selected to represent deficiencies common in older bridges.

Xiao, et al. [3] tested one as-built and three retrofitted bridge column footings under quasi-static loading. The footings were supported on elastomeric pads to simulate pile foundation flexibility.

The effects of in-situ foundation flexibility on the lateral load response and soil-structure interaction have been of interest for some time. Among the earlier field studies to quantify the influence of foundation flexibility on the lateral stiffness of bridges was

the work by Douglas and Reid [9] and by Werner [10]. Analytical studies showed that rocking of the footing can reduce the lateral stiffness by 50 percent (Saiidi and Orié [11]). The effect of soil flexibility on ambient vibration of bridges was studied by Crouse, et al. [12] and the damping and stiffness of the bridge system were evaluated. Modeling of the soil-structure interaction was the subject of several other studies [11, 13, 14]. These studies have shown that a stick model with lumped soil springs can adequately model the bridge response.

The available literature shows that the dynamic response of bridge pier systems (as opposed to single columns) has been rarely investigated experimentally. Also scarce, is information on the effect of foundation rocking on the dynamic behavior of both new and retrofitted bridge bents.

1.3 Objectives and Scope

The primary objective of the research presented in this report was to investigate the dynamic behavior of large-scale, two-column bridge piers supported on flexible footings using earthquakes simulated on a shake table and to determine the effects of footing flexibility on the force and deformation demand in footings, columns, the beam, and the joints. Elastomeric bearing pads represented the soil flexibility.

This was part of a more extensive study in which an innovative bridge pier system using carbon fiber reinforced plastics and reinforced concrete was developed and tested. Three quarter-scale structures, one with as-built footings on bearing pads, the second with retrofitted footings on bearing pads, and the third with fixed footings, were investigated. The first two were tested only in the linear range to avoid damage to the frame, but the

third pier was tested to failure. The focus of this report is on the effects of footing flexibility and the linear response of the three bents.

Chapter 2

SPECIMENS AND TESTING PROGRAM

2.1 Introductory Remarks

A two-column bent was constructed and tested with three different footing configurations, each with a different designation. This chapter briefly describes the design, construction, instrumentation, and testing of the specimens with particular emphasis placed on the footing design. Modeling and design of bearing pads to represent the soil flexibility are discussed in the next chapter.

2.2 Design of the Test Structure

A quarter-scale bridge bent with as-built as well as retrofitted footings was designed, constructed, and tested in the course of this research. The objective of the tests was to investigate the behavior of bridge footings during earthquakes, and to investigate the effect of footing flexibility on response of bridge bents for as-built as well as retrofitted footing configurations.

The specimen was tested with three different footing configurations. The resulting structures were named B2SA, B2SR, and B2SF, with B2S in each designation standing for bent with 2-columns, square, and the last letter in each representing the as-built, retrofitted, or fixed footings.

The pier was constructed to $\frac{1}{4}$ scale so that it could be accommodated on a 14.5 ft. x 14 ft. (4.4 m x 4.3 m) shake table. The beam and columns were innovative sections that consisted of reinforced concrete with nominal reinforcement. Unidirectional carbon

fiber reinforced plastic (CFRP) fabrics were used to act as primary reinforcement for flexure, shear, and confinement, except for plastic hinges where only mild steel reinforcement provided the flexural strength.

Figure 2.1 shows the bent dimensions, the composite layout, and the as-built footing dimensions. The lines within the elements show the direction of carbon fibers. Figure 2.2 shows beam and column cross-sections and Figs. 2.3 and 2.4 show column elevations and bar strain gage locations. Plastic hinges in the columns were offset by terminating the #5 bars some distance away from the column ends as shown in Fig. 2.2. The bent dimensions were chosen to reflect those of typical two-column highway bridge bents. The entire beam length and column middle regions were designed to remain elastic. Hence, composites were used for longitudinal reinforcement in these locations. Minimal longitudinal steel bars were provided for reinforcement of the beams and columns, also #4 stirrups were used at 9 in. (225 mm) spacing to reinforce the frame before the composites were installed. Two horizontal and two vertical layers of CFRP fabrics were provided at each joint on both sides of the bent for joint shear reinforcement. The joint shear design was based on the ACI 352 provisions [15]. The number of longitudinal CFRP layers was designed by trial and error based on specified material properties using strain compatibility and equilibrium.

2.3 As-Built Footing Design

The footings in B2SA were designed assuming a soil allowable bearing pressure of 4 kip/ft² (0.19 MN/m²) under gravity loading. The gravity loading was selected to produce an axial load index of approximately 0.1 assuming a specified concrete strength

of 4 ksi (28 MPa) (axial load index is the ratio of column axial load divided by the product of the gross section area and specified concrete compressive strength). A nearly square footing was designed with dimensions of 36 in. x 32 in. x 7 in (0.9195 m x 0.766 m x 0.179 m). The footing was approximately a 0.25 scale model of a typical prototype footing. The model footing contained #4 (ϕ 12.7 mm) bars placed along the footing bottom in each direction (Fig. 2.5).

2.4 Retrofitted Footing Design

Modern bridge specifications require that, under the most severe earthquake loading, no significant damage occurs in the footings and that plastic hinging be limited to columns. In addition to ensure ductile performance, there should be sufficient anchorage lengths for the column longitudinal bars, and no lap splices should exist at the plastic hinge of the columns.

Bridges designed before the 1970s generally do not fulfill these requirements. Hence, the as-built footings were retrofitted, taking into account additional demands due to plastic hinging in the columns, and their plan dimensions were increased to reduce the soil bearing pressure under the combined action of the vertical load and moment acting on the footing. Based on the plastic moment in the columns, the moment demand in the footing was found to be 1100 kip-in (124 kN-m). The footing was designed to resist 30% more than this moment to account for probable increase in column moment capacity due to material overstrength. Due to the relatively small plan dimensions of the as-built footing, the bearing pressure under the footing would be considerably higher than the allowable soil pressure. This deficiency of the as-built footing was addressed by

increasing the plan dimensions of the footing (Fig. 2.6). Note that the bent was loaded in the in-plane direction, hence, the main increase in dimensions of the footing was in the loading direction. A 5 in. (127 mm) thick overlay was placed on the as-built footing specimen. This provided the required nominal moment capacity of the footing section. The overlay was reinforced with a mat of steel bars running in both directions. The top mat, however, did not increase the moment capacity of the footing section appreciably, but provided for negative moment capacity. The percentage of the top mat was approximately 50% of the existing bottom reinforcement.

The new concrete was connected to the old footing using vertical and inclined steel dowels. The shear-friction method was used to calculate the size and spacing of the dowels. A coefficient of friction of 1 was assumed which required the hardened concrete surface to be intentionally roughened to full amplitude of $\frac{1}{4}$ in. (6 mm) in the model [16]. Number 3 (ϕ 9.5 mm) Grade 60 deformed steel dowels were used to connect the extended portion of the footing to the existing concrete. Inclined dowels are preferred rather than horizontal dowels because of constructability considerations. The dowels were embedded into the existing concrete to a depth of 5 in. (127 mm) (Fig. 2.6) (a minimum of 4.25 in (108 mm) was recommended by the epoxy manufacturer). The epoxy used was manufactured by the Simpson Strong-Tie Company, and design details for its use was obtained from ICBO-1998. Although an angle of 45 degrees is the most efficient angle, the dowels were inclined at an angle of 60 degrees to the vertical to provide sufficient embedment depth of the dowels inside the existing concrete (Fig. 2.7).

The top overlay concrete was anchored to the old concrete using #4 (ϕ 12.7 mm) Grade 60 vertical dowels, with an embedment depth of 4 in (101.6 mm) (Figs. 2.7).

Vertical plastic pipes were placed near each corner of each footing, to assist in fixing the footings to the shake table for the B2SF configuration in which the footings would be fixed.

Additional flexural reinforcement was designed as shown in Fig. 2.6. In addition to the inclined dowels used to connect the old concrete to the extensions, six # 4 (ϕ 12.7 mm) Grade 60 horizontal bars each on left and right faces were anchored to the existing concrete adjacent to the existing footing bottom bars. These bars were used to provide the required moment capacity of the section at the interface of the old and new concrete.

2.5 Construction of Test Specimen

The pier was constructed to $\frac{1}{4}$ scale so that it could be tested on the shake table. The construction was staged in several phases, with the footing, column and beam concrete poured separately. The formwork for the footing was assembled on a concrete platform. A layer of form release was applied to the formwork to prevent binding of the concrete. The footing bar mats were pre-assembled adjacent to the formwork, and placed in the forms. Four U-shaped lift hooks, made of ϕ 25.4 mm (#8) bars, were installed in the footings. The footing concrete was made at the laboratory. The pier formwork was constructed using wood, and concrete was poured in the footings first and later in the columns for convenience. The footing surface was leveled to a smooth finish. The footings were air cured.

The column formwork was completed after curing the footing concrete for a few days. The column forms were centered on the footings and braced to ensure they maintain their position in the horizontal and vertical directions during the concrete pour.

The transverse steel was adjusted, the column forms were assembled, and holes were drilled through the column forms to insert threaded rods used to measure curvatures. Finally, the beam form was built. A local ready-mix plant supplied the column and beam concrete. The columns were poured in approximately four lifts of 15 in. (381 mm) and mechanically vibrated during the pour on the inside and outside of the formwork to prevent voids. The columns and beam were moist cured for 7 days prior to removal of the formwork.

2.6 Material Properties

The concrete used in the pier was normal-weight concrete with a maximum aggregate size of 3/8 in. (10 mm). Portland cement type I was used. The target concrete compressive strength was 5 ksi (34 MPa), while the actual strengths were 6.26 ksi (42.8 MPa) in the columns and 5.29 ksi (36.1 MPa) in the beam on the day of testing B2SF. The data were measured in accordance with ASTM C-39. Table 2.1 shows the measured concrete properties. The concrete was air cured, and subsequently the surface of the concrete was prepared for laminate application. The steel bars were of Grade 60. The measured yield stresses are shown in Table 2.2.

The Mitsubishi CFRP product, Replark Type 30, was used. First the surface was ground using a disk grinder, then putty (supplied by the manufacturer of the composites) was applied to smooth out rough spots. Next, a layer of resin undercoat was applied followed by a layer of carbon fiber sheet. This process was repeated for all the layers. The composite installation was completed by application of a resin overcoat. Any air bubbles trapped beneath the laminate were repaired by injecting epoxy into the voids.

The specified CFRP elastic modulus in the fiber direction was 33,400 ksi (228 Gpa), while its tensile strength along the fiber direction was 493 ksi (3.365 GPa). Coupons were also tested as part of this study, and the lamina elastic modulus in the fiber direction was found to be 38,400 ksi (262.3 Gpa), while its tensile strength along the fiber direction was 379.8 ksi (2.593 GPa). The measured lamina elastic modulus perpendicular to the fiber direction was 509.6 ksi (3.48 GPa) and its tensile strength perpendicular to the fiber direction was 1.76 ksi (12 MPa).

2.7 Instrumentation

The test specimen was extensively instrumented to record bar strains, CFRP strains, column curvature, column displacement, lateral forces, and the vertical load. The test data were recorded on a Pacific data acquisition system at a rate of 160 samples per second.

Sixteen strain gages were used in the as-built footings and 40 strain gages were used in the retrofitted footings. Figures 2.3 to 2.6 show a sample of the strain gage locations on the bars. The strain gages were manufactured by Tokyo Sokki Kenkyujo Co., Ltd. of Japan. The steel reinforcement was instrumented with 0.4 in. (10 mm) strain gage model (YL-10-5L).

Curvature was measured using a series of *Novotechik* transducers. Five 0.375 in. (9.5 mm) threaded rods were installed in the plastic hinge regions of each column. The threaded rods begin at 7 in. (178 mm) from the as-built footing elevation and continue up to 17 in. (432 mm) above the footing. The rods support the ends of the *Novotechnik* transducers, allowing curvature to be calculated based on the displacements measured by

the transducers. Figure 2.8 shows the location of the threaded rods. A total of eight *Novotechnik* transducers were installed along each column surface with four on either side.

In B2SA and B2SR, two *Novotechnik* transducers were used to measure uplift of each footing, and one was used to measure the horizontal displacement of each footing relative to the table when the flexible footing tests were done.

Load cells were used to measure the vertical loads applied through the axial load rods (Fig. 2.9). The axial loads were measured by placing load cells under the hydraulic jacks above the loading frame attached to the beam. Five accumulators were placed in line with the hydraulic jacks to minimize axial load variation. The lateral loads were measured by a load cell attached to the steel link connecting the loading frame with the mass rig. Column absolute displacement was measured relative to the laboratory wall using a Temposonic transducer attached to the top of the test specimen, at the level of the mass rig connection, as shown in Fig. 2.9. The shake table displacement was measured by an internal transducer, which allowed the relative column displacement to be calculated as the difference between the absolute bent top displacement and table displacements.

2.8 Program of Experimental Studies

2.8.1 Test Setup

Each test specimen was centered and supported on neoprene bearing pads attached to the shake table. Bearing pads were also placed on the footing sides, and they were supported by steel brackets, which were bolted to the shake table (Fig. 2.9). In

many shake table tests, the mass is placed on top of the structure to be tested. A supporting structure must be included to prevent damage to the shake table system if complete column and mass collapse occur. The setup used here allows the vertical load effect of mass on the structure to be simulated using prestressed vertical rods attached to the shake table, and the horizontal inertial effect of the load on the structure to be represented using the mass rig. The lateral loading of the specimen was accomplished through the mass rig, which consisted of a pinned steel frame mechanism supporting concrete blocks. The design of the mass rig is outlined in Ref. 17. The mass rig was connected to the specimen by the loading frame and a steel plate with a pinned circular steel tube. The other end of the tube was pinned to the mass rig by a steel plate. The mass rig supported two concrete blocks, each weighing 20 kips (89 kN). In addition, the mass rig frame weight produced an equivalent lateral inertial force of approximately 20 kips (89 kN), hence the total lateral inertial mass provided was approximately 60 kips (267 kN). Also the mass of the link, load transfer girder, and the cap beam provided 3 kips (13 kN), thus making the total inertial mass 63 kips (280 kN). After the mass rig link was connected to the specimen, an axial load of 63 kips (280 kN) was applied through the hydraulic jack system. Hence, using this system, the effect of having a weight of 64 kips (285 kN) on the specimen was achieved.

The hydraulic system consisted of ten hydraulic jacks connected to a pump and accumulator in series. The pump was engaged to provide the axial load, and the accumulator was used to minimize the axial load fluctuation. The axial load rods were attached to steel L-sections, which in turn were bolted to the footing brackets.

2.8.2 Testing Program

The earthquake history used to drive the shake table was the January 17, 1994 Northridge earthquake as measured at the Sylmar Hospital. This record was chosen due to it being representative of a typical near-field earthquake in the western United States. Furthermore, analytical studies showed that this record would lead to high ductility demand. Since the test specimen was a scaled model of a prototype bent, the time axis of the earthquake record had to be scaled to create a response in the test specimen that would parallel the prototype column. Hence, the earthquake time step was scaled by a factor of 0.5 (the square root of the scale factor of 0.25) to account for the differences between the prototype and specimen vibration periods.

Tuning of the shake table system was accomplished through low level testing of the specimen prior to the test program. The tuning was necessary to improve the correlation between the target and the actual table acceleration histories. The strong motion accelerogram was input into the table control system, which converted the accelerogram into a drive file that operates the shake table actuator. The shake table motion, without the specimen attached to the table, accurately represents the input strong motion accelerogram. However, the table response is affected by the stiffness and mass of the test specimen and tends not to model the input motion precisely. The difference between the input and actual table acceleration must be corrected to ensure that the shake table adequately simulates the earthquake. Low level testing is completed through applying a series of random vibrations to the shake table, which allows the operator to adjust the response of the system. The amplitude of this vibratory motion is substantially below the predicted yield point of the specimen to ensure no yielding of the model. The

goal of the tuning process was to preserve the low frequency response of the input motion in the testing motion.

The testing was completed by applying scaled versions of the strong motion accelerogram. The intent of the tests in B2SA and B2SR was to study the linear response and to avoid damage so that the specimen could be saved for testing with fixed base. As a result, the maximum amplitude of the input motions was limited and the increments of the peak input accelerations were small. The final run in testing of B2SA and B2SR was selected during the experimental studies using a general guideline of keeping the critical longitudinal bar strains below two-thirds of their yield strain.

The testing of B2SA consisted of six events, as shown in Table 2.3. The peak table acceleration for each event was incremented by one-tenth of the Sylmar peak acceleration. The peak acceleration that was applied to the as-built specimen was limited to 0.6 times the Sylmar acceleration. The testing of B2SR consisted of four events, as shown in Table 2.4. In this model, the peak acceleration was limited to 0.4 times the Sylmar acceleration to prevent premature yielding in the plastic hinges. This specimen was stiffer than B2SA and attracted larger lateral forces. As a result, bar strains were higher and testing had to be stopped at 0.4 x Sylmar instead of 0.6 x Sylmar in B2SA. Finally, the bearing pads were removed, the footings were fixed to the shake table, and the bent was tested to failure (model B2SF), according to the scheme shown in Table 2.5. The peak table acceleration increments initially were one-tenth of the Sylmar peak acceleration, in order to capture important phenomena like cracking and sequential yielding of the plastic hinges. After major yielding had been initiated at about 0.6 x Sylmar, the increments were increased to one-fifth of Sylmar. For the last few runs, the

increments were increased to one-quarter of Sylmar since, by then, all the plastic hinge zones had completely yielded. Because of concerns over the stability of the specimen, a motion with peak acceleration of 1.9 x Sylmar was applied after run 11 (Table 2.5). The specimen withstood this motion and the lateral load capacity did not degrade. Finally a motion with peak acceleration of 2 x Sylmar was simulated, during which the lateral load capacity degraded and the CFRP jacket in one of the plastic hinges ruptured.

Chapter 3

MODELING SOIL FLEXIBILITY

3.1 Introductory Remarks

The effect of foundation flexibility was simulated by placement of neoprene elastomeric bearing pads below and on the sides of the footings. The bearing pad material properties and dimensions were selected based on the required footing horizontal and vertical stiffnesses, which were found by using the Schmertmann Strain Factor Method [18]. This chapter describes the steps involved in designing the bearing pads for the bent, which includes finding a representative soil stiffness, evaluating the bearing pads properties, and finally, designing the number of bearing pads.

3.2 Schmertmann's Method

It was assumed that the footings rest on compacted, cohesionless, dense sand. In order to find the soil stiffness, the stress-settlement relationship of the soil is needed. This was found by using Schmertmann's Strain Factor method [19], a widely recommended procedure in many design manuals. The procedure has been found to duplicate experimental stress-settlement relationships well [20-23]. This method provides a logical means of accounting for the variations in the stress-dependent, nonlinear stiffness of sand as a function of depth. The analysis is based on the assumption that the distribution of vertical strain below the footing is compatible with linear elastic half space.

3.2.1 Soil Vertical Stiffness

According to Schmertmann's method, the settlement, δ_v , of a uniformly loaded surface footing can be written as

$$\delta_v = C_p \sum \varepsilon_v \Delta z = C_p * C_1 \sum \left(\frac{\Delta p I_z}{2 * (1 + \nu) * G} \right) * \Delta z \quad (3-1)$$

in which ε_v = the vertical strain in the sublayer in the foundation soil; C_p = the correction factor, Δp = the net applied footing pressure given by $(F_v/B - \sigma_0)$; F_v = applied footing load /L where L is footing width perpendicular to plane of analysis; σ_0 = the overburden pressure at the base of the foundation; Δz = the thickness of the sublayer; I_z = the vertical strain influence factor; G = the secant shear modulus of the sublayer; B = width of footing parallel to plane of analysis; and ν = poisson's ratio of the soil. C_1 is a correction factor to account for strain relief from embedment. It is $(1 - 0.5\sigma_0/\Delta p)$ and should be at least 0.5. An iterative procedure adopted from Ref. 19 to account for the stress-dependent nonlinear foundation soil is presented below.

(1) Divide the soil beneath the foundation into a number of sublayers to a depth below the footing of up to about four times the width B and assume a certain value of F_v .

(2) For each layer, assume the initial secant shear modulus, G , to be a fraction of G_{\max} , typically $1/2 G_{\max}$. Here, G_{\max} is the maximum shear modulus at a low shear strain; it may be computed using the equation given by Seed and Idriss [24].

$$G_{\max} = 218.8 \cdot (K_2)_{\max} \cdot \sqrt{(\sigma_m)} \quad (3-2)$$

Where $(K_2)_{\max}$ = the constant that depends on the relative density of the soil and σ_m = the mean normal stress of the layer. G_{\max} and σ_m are given in kPa and σ_m is the combined

stress due to the overburden and the load. The average load induced stresses in the sublayer are computed using a 2:1 spread as often used in foundation engineering.

(3) Compute the vertical strain, ε_v , in each sublayer using the terms that are within the brackets in Eq. 3-1.

(4) Estimate the average shear strain, γ_{ave} , in the sublayer using Eq. 3-3

$$\gamma_{ave} = (1 + \nu) \cdot \varepsilon_v \quad (3-3)$$

and the shear modulus given for this shear strain from the shear modulus reduction curve by Seed and Idriss given below (γ is shear strain of sublayer, G/G_{max} cannot exceed 1 and cannot be less than 0.08):

$$\frac{G}{G_{max}} = 0.063577 - 0.1357 \cdot 10^\gamma + .16168 \cdot 10^{2\gamma} + 0.034663 \cdot 10^{3\gamma} \quad (3-4)$$

(5) If the difference between the assumed (Step 2) and computed (Step 4) shear modulus is not within 5%, repeat Steps 2 through 4. If convergence occurs in all sublayers, then compute the foundation settlement, δ_v , using Eq. 2-1.

The entire nonlinear vertical stress-settlement curve can be obtained by increasing the value of F_v . The curve is, of course, limited by the ultimate bearing capacity of the foundation. The secant stiffness of the plot corresponding to the gravity load induced footing stress can be found. The stiffness can be scaled to suit the model footings, and it can be used to design the bearing pads.

The influence factor I_z is based on approximation of strain distribution for square or axisymmetric footings observed in cohesionless soil. Cohesionless soil is similar to an

elastic medium such as the Boussinesq distribution. The peak value of the influence factor, I_{zp} , is

$$I_{zp} = 0.5 + 0.1 \cdot \frac{\Delta p^{\frac{1}{2}}}{\sigma'_{Izp}{}^{\frac{1}{2}}} \quad (3-5)$$

$$\sigma'_{Izp} = 0.5 \cdot B \cdot \gamma' + D \cdot \gamma' \quad (3-6)$$

Where σ'_{Izp} = effective overburden pressure at the depth of I_{zp} , N/m^2 ; γ' = effective unit weight (wet soil unit weight γ less unit weight of water), N/m^3 ; D = excavated or embedded depth, m; I_z may be assumed to increase linearly from 0.1 at $z = 0$ to I_{zp} at $z = 0.5 \cdot B$; and to decrease linearly to 0 at $z = 2 \cdot B$. A computer program in FORTRAN 77 language was developed for calculating the footing vertical stress-settlement relationship.

3.2.2 Soil Horizontal Stiffness

A similar procedure to the one described above was adopted to arrive at the horizontal stress-displacement relationship. The lateral movement, δ_h , is given by

$$\delta_h = \sum \gamma_h \Delta z = \sum \left(\frac{F_h}{B} \right) \cdot \left(\frac{I_h}{G} \right) \cdot \Delta z \quad (3-7)$$

Where γ_h = the shear strain in the sublayer and I_h = the shear strain influence factor. Note that the effect of soil on the footing sides on the footing response was neglected (this is a conservative assumption, since it would lead to larger footing displacements). Also, phenomena like erosion could cause the footing, although initially embedded in the soil, to be at ground level. The shear strain influence factor, which is similar to Schmertmann's vertical strain influence factor, has been deduced from the elastic half

space solution. For an axisymmetric footing ($L=B$), if z is the depth below the footing with respect to the base of the footing and $a=z/L$, I_h is given by the following equation:

$$I_h = \frac{2}{\pi} \cdot \left[\cot^{-1}(4 \cdot a \cdot \sqrt{0.5 + a^2}) - \frac{a}{4 \cdot (0.25 + a^2) \cdot \sqrt{0.5 + a^2}} \right] \quad (3-8)$$

The iterative procedure outlined above has been adopted to arrive at the nonlinear F_h - δ_h relationship. The limit to this relationship is imposed by the interface friction force given by $F_v \tan \delta_f$ in which δ_f is the interface friction angle between the foundation soil and the base. A computer program in FORTRAN 77 was written for calculating the footing horizontal stress-displacement relationship.

3.3 Equivalent Soil Stiffness for the Model

Dimensions of the footings for the as-built and retrofitted models, as well as the corresponding prototypes, are listed in Table 3-1. The footing retrofit design was described in Chapter 2. Since the prototype (full-scale) footings are assumed to be resting on cohesionless soil, the load-settlement relationships were found for this case and were scaled down to suit the model footings.

Based on the footing dimensions and the vertical dead load on the footing, the footing normal and shear stresses on an equivalent full-scale (prototype) footing were found as follows. These values were used in the computer programs described in the previous section to obtain the equivalent soil stiffness for the prototype footing. The values were then scaled to obtain soil stiffnesses for the specimen.

3.3.1 Average Normal and Shear Stresses on Footings

In the scaling process, the stresses were not scaled. Therefore, the average bearing and shear stresses in the model footings were the same as those in the prototype. Based on the column axial load index of 0.1, the specified concrete strength, and the footing dimensions shown in Table 3.1, the normal stress in the footings under vertical load was 3.77 ksf (0.181 MPa) and 2.14 ksf (0.102 MPa) for the as-built and retrofitted footings, respectively.

The average shear stress was estimated assuming a maximum lateral acceleration of 0.9 g due to earthquake loading. As a result, the footing shear stress was 0.9*footing normal stress. For the as-built footings, the shear stress was 3.39 ksf (0.162 MPa) and for the retrofitted footings, the shear stress was 1.93 ksf (0.0924 MPa).

3.3.2 Evaluation of Soil Stiffness

The stress-displacement relationships in the vertical and horizontal directions were found for the prototype footings using Schmertmann's strain factor method and were plotted (Fig. 3.1 to 3.4). In addition to the footing dimensions, Table 3-1 shows the average footing dimensions (B') and the soil depth to the bottom of the footing (D) used in the analysis. Only the values for prototype footings are given because these parameters were not needed for the model footing.

For the as-built footing at an average vertical stress of 3.77 ksf (0.181 MPa), the settlement is 0.141 in (3.58 mm), and the secant soil stiffness is 26.7 ksf/in. (50.6 kN/m²/mm). The vertical soil stiffness in the retrofitted footing is 34 ksf/in. (63.7 kN/m²/mm) and it was found for a normal stress of 2.14 ksf (0.102 MPa) in Fig. 3.2.

Using Figs. 3.3 and 3.4, the horizontal soil stiffnesses were found for the stresses discussed in the previous section. At a stress of 3.39 ksf (0.162 MPa), the horizontal secant soil stiffness for the as-built footing is 17.93 ksf/in. (33.6 kN/m²/mm). For the retrofitted footing the soil stiffness is 24.35 ksf/in. (46.2 kN/m²/mm) for an average shear stress of 1.93 ksf (0.0924 MPa).

The stiffness values used in structural modeling are based on force and not stress. Therefore, the aforementioned soil stiffnesses that are available in stress-displacement form were first converted to horizontal and vertical footing stiffnesses for the prototypes by multiplying them by the footing plan view areas. The results are summarized in the right two columns of Table 3-1. To obtain the footing stiffness in the model, the values for the full-scale footings were multiplied by the scale factor of 0.25. The results are shown in Table 3-1.

3.4 Bearing Pads

Elastomeric pads with durometer rating of 50 and size of 10 in. x 10 in. x 2 in. (254 mm x 254 mm x 50 mm) were used under the footing. Similarly, pads of size 10 in. x 10 in. x 1 in. (254 mm x 254 mm x 25 mm) were placed along each vertical face of the footing perpendicular to the plane of the bent to simulate the effect of soil flexibility.

3.4.1 Bearing Pad Stiffness

The bearing pads were tested in an Instron testing machine to determine their normal stiffness. The measured compression stiffness of the 1-in. (25-mm) thick pads was 246 k/in. (43.1 kN/mm) and that of the 2-in. (51-mm) thick pads was 67.7 k/in. (11.9

kN/mm). These values were the tangent stiffnesses (tangent to the initial part of the stress-displacement plot).

The bearing pad shear stiffness was determined based on shear modulus values reported in Ref. 25 and 26. For bearing pads with durometer rating of 50, the shear modulus of elasticity is 92.8 psi (640 kPa) according to Ref. 25. The shear modulus given in Ref. 26 is 145 psi (1000 kPa) with no reference to durometer rating. A shear modulus of 100 psi (690 kPa) was used in this study. Based on this value, the shear stiffness is 10 k/in. (1.75 kN/mm) and 5 k/in. (0.8476 kN/mm) for the 1-in. (25-mm) and the 2-in. (50-mm) thick pads, respectively.

3.4.2 Bearing Pad Design

The pads were designed by matching the vertical and horizontal footing stiffness, K_v and K_h with those of the pads. Note that when a match between the footing stiffness and the pads in the vertical direction is achieved, the rotational footing stiffness is also matched. This is because the rotational footing stiffness is provided by the vertical stiffness of the pads. The vertical and horizontal stiffness of the footings are related to the number and stiffness properties of the bearing pads as shown in the following equations:

$$K_v = C_2 * N_h + S_1 * N_v \quad (3-9)$$

$$K_h = C_1 * N_v / 2 + S_2 * N_h \quad (3-10)$$

Where K_h = Shear stiffness provided by bearing pads for each footing; K_v = Compression stiffness provided by bearing pads for each footing; C_1 = stiffness of one 1-in. (25-mm)

pad in compression; S_1 = stiffness of one 1-in (25-mm) pad in shear; C_2 = stiffness of one 2-in (50-mm) bearing pad in compression; S_2 = stiffness of one 2-in (50-mm) pad in shear; N_h = number of horizontal pads under each footing; and N_v = total number of vertical pads on the sides of each footing.

Figure 3.5 shows a schematic view of a footing with reaction forces on the pads under vertical loads. Under lateral loading, the pads only on one side of the footing are effective in any given direction as shown in Fig. 3.6.

Based on the dimensions of the footings and the size of the pads, nine 2-in. (50-mm) pads were placed at the bottom and three 1-in. (25-mm) pads were placed on each side of each as-built footing. For the retrofitted footings, 12 2-in. (50-mm) pads were placed at the bottom and four 1-in. (25-mm) pads were placed on each side of each footing. Figure 3.7 shows the side view of one of the retrofitted footing with the pads highlighted for clarity.

In selecting the number and size of the pads, it was necessary to use the same pad thickness for the ones under the footings and the same pad thickness for the side pads. Considering these constraints the resulting footing stiffness deviated from the target values. The last two rows in Table 3.1 show the provided stiffnesses. It can be seen that the vertical stiffness in the retrofitted footing was significantly lower than the target value. Nonetheless, because it is the horizontal stiffness, which is of primary interest under earthquake loading, and because the provided horizontal stiffnesses were within 20 percent of the target values, the bearing pad design was considered to be acceptable.

Chapter 4

EFFECTS OF FOUNDATION FLEXIBILITY ON RESPONSE

4.1 Introductory Remarks

The earthquake simulation program was presented in Chapter 2. Using the measured data, the effect of foundation flexibility was evaluated on several critical parameters. The response parameters that were reviewed and presented in this report included the overall load-displacement response, steel bar strains, composite fabric strains, footing displacements, and footing rotations. This chapter presents the results with a focus on the measured foundation flexibility effects. A more comprehensive report on the response of the test structures and an extensive analytical study of the bents is in progress at the time of this writing and will be published in the future.

4.2 Load-Displacement Response

The overall effect of foundation flexibility can be observed on the lateral load-displacement response of the bents. The envelopes of the measured hysteresis curves were compared in Fig. 4.1 to assess the effect of footing flexibility. The envelopes for B2SA and B2SR are the complete results for all the runs. The envelope for B2SF shows the results only for the first four runs because the response for the remaining runs in this bent were associated with yielding of steel, which did not apply to B2SA and B2SR. It can be observed that the response of all three frames was nearly linear for the amplitude of the earthquakes that were simulated. This was intentional to avoid damage in the beam and the columns during B2SA and B2SR testing and allow for the use of the frame

for three different footing setups. The figure also shows that the stiffness (the slope of the envelopes) increased when the footing was retrofitted. The chord stiffness for the last run in B2SR was 23 percent higher than the stiffness of B2SA for the same peak displacement. It is also interesting to note that the stiffness of B2SF, which was on fixed footings, was only slightly higher (by less than 3 percent) than that of B2SR. It is believed that the bent cracked in B2SR, and the increase in footing stiffness in B2SF, was offset by the softening of the frame, thus leading to nearly the same stiffness for B2SR and B2SF.

4.3 Column Moments

To estimate the moment demand in different test models, the maximum measured longitudinal bar tensile strains were compared. The bar strains were grouped for the bottom and the top of the columns. Within each group, the strains in the plastic hinge and in sections adjacent to the plastic hinges were evaluated.

Figures 4.2 and 4.3 show the measured peak tensile strains in the bottom and top plastic hinges of the left column, respectively. Prior to earthquake simulations, small compressive strains had been developed in the bars, but these strains are not shown in the figures. Both figures indicate that the strains in B2SA were considerably lower than the strains in B2SR and B2SF. The peak strains in the retrofitted model (B2SR) were also significantly lower than those in the fixed model. There was generally a large difference between the magnitude of strains at the top and bottom plastic hinges. In the bottom plastic hinge under 0.4xSylmar, the peak strain in the as-built model was less than two percent of the fixed model strain, and the peak strain in the retrofitted model was only 17

percent of that in the fixed model. For the same earthquake in the top plastic hinge, the as-built and retrofitted strains were 39 and 58 percent of the fixed-base strains, respectively. The foundation flexibility in both the as-built and retrofitted bents reduced the peak strains, but the reduction was lower at the top of the column indicating that the effect of footing flexibility is particularly pronounced on the moments at the base of the columns. The effect of footing flexibility on strains and the trends in comparing the strains at the top and bottom of the columns can also be observed in the measured tensile maximum strains adjacent to plastic hinges (Figs. 4.4 to 4.8).

4.4 Beam Moments

Beam bar strains were measured at the face of the columns. Recall that only nominal steel reinforcement was placed in the beams because CFRP fabrics were the main reinforcement. The bar strains under vertical loading and prior to earthquake simulations were small and inconsequential and were not, therefore, shown on the graphs. Figures 4.9 to 4.11 show that the beam bar strains in the as-built model were lower than the strains in the retrofitted and fixed models. The peak strains in the retrofitted model were also generally lower than those in the fixed bent. Some exceptions are noted for motions with 0.2 x Sylmar or less. It is believed that the beams in the retrofitted model cracked and softened the system, hence, the strains in the fixed model were relatively small under smaller motions. The relative values of beam bar strains for different support conditions are comparable to those of column tops, indicating that the footing flexibility effect is less pronounced as the distance to the footings increases. For the motion with 0.4 x Sylmar, the average as-built model peak strain for the data shown in the figures was

46 percent of the fixed model strain. For the same motion the average retrofitted model strain was 71 percent of the fixed model strain. These percentages are higher than those of top column plastic hinges. Because footing flexibility reduced the beam bar strain in B2SR by only 29 percent, the full retrofit of the beam assuming fixed footings may be appropriate.

4.5 Joint Forces

Vertical and horizontal strain gages were installed on CFRP fabrics at the centers of beam-column connections. Under reversed cyclic loads, beam column joints are subjected to cyclic diagonal stresses as the flexural forces from the beam and column act on the joint. Using the strain data the joint shear and the diagonal tension forces can be estimated.

The variation of joint strain data is shown in Figs. 4.12 to 4.14. It is clear in the figures that the relative values of the curves for the three models are similar to those of beam bar strains. Also evident are the trends in reduction of strains due to footing flexibility. Because the joint forces in the retrofitted model (B2SR) are relatively close to those of the fixed model (B2SF), a full retrofit design of the joint may be warranted.

4.6 Moment in Footings

The effect of footing flexibility on the maximum footing bar tensile strains was studied by comparing the measured data for the footing bottom bars measured at the face of the columns. The instrumented bars ran parallel to the plane of the bent. Note that in B2SF, the footings were fixed to the base and no measurement was taken for the footing

bars. Prior to earthquake simulations, the footings were subjected to vertical loads that led to some strains. Compared to the strains caused by earthquakes, the strains under vertical load were significant and hence included in the plots. Figures 4.15 to 4.18 show that as-built footing bar strains were lower than those of the retrofitted footings. The higher overall stiffness of B2SR increased the forces and hence led to larger strains in the footing bars. On the average, the B2SA bar strains were 25 percent lower than those of B2SR. The plots generally suggest that the as-built bar strains could reach and exceed the retrofitted footing bar strains under earthquakes with larger amplitudes, thus necessitating a complete retrofit of the as-built footings.

4.7 Footing Displacements and Rotations

The horizontal and vertical movements of the footings relative to the shake table were measured during earthquake simulations. The vertical displacements were measured at the edge of the footings, thus allowing for estimating the footing rotations by neglecting the bending of the footings.

Shown in Fig. 4.19 is the average of peak footing horizontal displacements for B2SA and B2SR. For the same lateral force, the displacement in B2SA was higher because of the lower stiffness of the footings in B2SA. At a footing displacement of 0.1 in. (2.5 mm), the stiffness of B2SR is approximately 52 percent larger than that of B2SA. Theoretically, the footing stiffness in B2SR was 68 percent higher than that of B2SA (Table 2.1).

The measured footing rotations are shown in Fig. 4.20. The rotations are based on the vertical displacements divided by the distance of the transducers. The data for the

left footing in B2SR could not be obtained because one of the vertical transducers malfunctioned. Considering the closeness of the right and left footing results for B2SA, it is reasonable to assume that the curve for the right footing of B2SR is representative of rotation for the left footing. The difference between the rotations of B2SA and B2SR was relatively small. At a rotation of 0.005 radians, the rotational stiffness of footings in B2SR was only 16 percent larger than that of B2SA.

4.8 Contribution of Footing Displacement to Total Response

The top lateral displacement of B2SA and B2SR was increased due to the flexibility of the footings. Both horizontal displacement and rotation of the footings contributed to lateral displacement at the top of the bents. While the contribution of the footing displacement is directly transferred to the top of the frame and can be readily quantified, determining the top displacement caused by the rotation of the footing cannot be directly determined and would require a combination of analytical and experimental studies. Another indirect approach to determine the top displacement due to footing rotation would be to compare the force-displacement envelopes for the three models (Fig. 4.1) to isolate top displacement due to footing flexibility, and subtract from this displacement the horizontal displacement of the footings. This method would be appropriate for a completely linear system. However, some of the strain data indicated that the frame cracked during the testing of B2SR, and the frame in B2SF had softened. This is clearly evident in Fig. 4.1 in which the envelopes of B2SR and B2SF are close. There is hence no reliable method to extract the effect of footing rotation on the measured top displacement.

The effect of footing displacement is shown in Figs. 4.21 and 4.22 for B2SA and B2SR, respectively. For the maximum force in B2SA, 20 percent of the top displacement was due to the average of footing horizontal displacement. In B2SR, the contribution of horizontal footing displacement to the top displacement was 19 percent.

4.9 Design Implications

Based on the discussions in previous sections the following important design issues were noted:

- (1) When footing flexibility is included, the structure has lower stiffness. The reduced stiffness leads to a higher lateral yield displacement and a higher ultimate displacement. Because the yield displacement is more sensitive to footing flexibility, this will reduce significantly the apparent displacement ductility capacity of the structure compared to a fixed structure.
- (2) Footing flexibility reduces the moment demand in the columns. This effect is particularly pronounced at and near the base of the columns. A reduced moment demand potentially implies a reduction in retrofit detailing requirements for substandard columns such as those with lap splices, inadequate confinement, or insufficient shear reinforcement. This reduction could lead to substantial savings in column retrofit cost.
- (3) While the data for beam moment demands suggest a reduction due to footing flexibility, the reduction is not substantial leading to the conclusion that full retrofit of the beam may be warranted.

(4) When the structure was supported on flexible footings, joint shear forces were reduced. However, the amount of reduction was not sufficiently large to justify a waiver of seismic retrofit requirements for joint. Guidelines developed for retrofit of beam column joints in bents supported on fixed footings should be used.

Chapter 5

SUMMARY AND CONCLUSIONS

5.1 Summary

This report presents a part of an experimental study on the seismic response of two-column bridge bents that was focused on (1) effects of foundation flexibility on the linear dynamic response; (2) adequacy of using carbon fiber reinforced fabrics as the primary reinforcement; and (3) performance of bents with shifted plastic hinges in columns. The part of the study described in this report is on the foundation flexibility effects.

An exploratory study to determine the influence of foundation rocking and horizontal displacement on the shake table response of a quarter-scale two-column bridge bent was conducted. Several innovative details and designs were used in the columns and the cap beam, but the footings represented typical substandard and retrofitted spread footings. The structure was tested in three conditions. In the first condition, the structure was designated as B2SA and the footings were substandard isolated footings that were allowed to rock and displace laterally. In the structure in the second test setup, B2SR, the footings were retrofitted by enlarging them, increasing their thickness, and adding more steel reinforcement. The footings in B2SR were also supported on flexible footings that allowed for rocking and horizontal displacement. The structure in the third testing configuration, B2SF, was fixed to the shake table and tested under increasing amplitudes of simulated earthquakes until it failed.

In B2SA and B2SR, the foundation flexibility was modeled in the tests using elastomeric bearing pads that were designed to represent the stiffness of spread footings supported on compacted cohesionless soil with medium density. The tests with flexible footings were conducted in the elastic range, but the fixed-base model was tested to failure. The Sylmar record of the 1994 Northridge earthquake was simulated on the shake table. The data showed that for the same input earthquake intensity, the maximum steel bar tensile strain near the base of the columns in an unretrofitted flexible footing was only 2 percent of the strain in the fixed frame. When the footing was retrofitted but was on flexible supports, the maximum steel strain increased but was still only 17 percent of the strain in the fixed frame. The effect of footing flexibility on the bar strains in the plastic hinges near the top of the column was less drastic, but was substantial. The maximum tensile bar strains at the top plastic hinges in B2SA and B2SR were 39 and 58 percent, respectively, of the maximum strain in B2SF. Foundation flexibility also reduced the strains in the footing bars, the joints, and the beam bars, although the extent of reduction was less than that of column bases.

5.2 Conclusions

Based on the results presented in this study the following conclusions may be drawn:

- (1) The use of elastomeric bearing pads was an effective mean to simulate footing flexibility effects.

- (2) All the internal forces were reduced because of footing flexibility. However, the extent of reduction was most pronounced at and near the base of the columns and was less substantial in beam bars.
- (3) When footing flexibility is included, the structure has lower stiffness. The reduced stiffness leads to a higher lateral yield displacement and a higher ultimate displacement. Because the yield displacement is more sensitive to footing flexibility, this will reduce significantly the apparent displacement ductility capacity of the structure. This should be taken into account in judging the displacement capacity of bents on flexible footings.
- (4) The reduction in column moment demand due to footing flexibility potentially implies a reduction in retrofit detailing requirements for substandard columns such as those with lap splices, inadequate confinement, or insufficient shear reinforcement. This reduction could lead to substantial savings in the cost of column retrofit.
- (5) While the data for beam moment demands suggest a reduction due to footing flexibility, the reduction is not sufficiently pronounced and, hence, full retrofit of the beam may be warranted.
- (6) When the structure was supported on flexible footings, joint shear forces were reduced. However, the amount of reduction was not sufficiently large to justify a waiver of seismic retrofit requirements for joints. Guidelines developed for retrofit of beam column joints in bents supported on fixed footings should be used.

REFERENCES

- (1) Priestley, M., F. Seible, and M. Calvi, Seismic Design and Retrofit of Bridges, "Wiley-Interscience, 1996.
- (2) Wipf, T., F. Klaiber, and F. Russo, "Evaluation of Seismic Retrofit Methods for Reinforced Concrete Columns," Report 97-0016, Multidisciplinary Center for Earthquake Engineering Research, University of Buffalo, New York, December 1997.
- (3) Xiao, Y., M.J.N. Priestley, and F. Seible, "Seismic Assessment and Retrofit of Bridge Column Footings," *ACI Structural Journal*, 93(1), January 1996, pp. 79-94.
- (4) Saiidi, M., D. Sanders, and S. Acharya, "Seismic Retrofit of Spread Footings Supporting Bridge Columns With Short Dowels," Journal of Construction and Building Materials, Vol. 15, No. 4, June 2001, pp. 177-186.
- (5) McLean, D. I., and M.L. Marsh, "Seismic Retrofitting of Bridge Foundations," *ACI Structural Journal*, 96(2), March 1999, pp 174-182.
- (6) Celebi, M. and I. Okawa, Ed., *Proc. of the UJNR Workshop on Soil-Structure Interaction*, US Geological Survey Rep., 1999, pp. 99-142.
- (7) Fukuwa, N., M.A. Ghannad, J. Tobita, and R. Nishizaka, "Analytical And Experimental Studies On The Effect Of Soil-Structure Interaction On Damping, Natural Frequency And Effective Input Motion Of Buildings," *Proc. of the UJNR Workshop on Soil-Structure Interaction*, US Geological Survey Rep., 1999, pp. 99-142.
- (8) Acharya, S., M. Saiidi, and Sanders, D. "Seismic Retrofit of Bridge Footings and Column Footing Connections," *Rept. CCEER-95-7*, Engineering Research and Development Center, College of Engineering, University of Nevada, Reno, 1995.
- (9) Douglas, B., and W. Reid, "Dynamic Tests and System Identification of bridges," Journal of Structural Engineering, ASCE, Vol. 108, No. 10, October 1982, pp. 2295-2312.
- (10) Werner, S.D., "Seismic Evaluation Procedure for Short Bridges," Proceedings, 3rd Caltrans Seismic Research Workshop, Sacramento, California, June 1994.
- (11) Saiidi, M., D. Orie, and B. Douglas, "A Microcomputer CAD System for Seismic Design of Regular Highway Bridges," Ninth Conference on Electronic Computation, Birmingham, Alabama, February 1986.

- (12) Crouse, C., B. Hushmand, and G. Martin, "Dynamic Soil-Structure Interaction of Single-Span Bridge," *Int. Journal of Earthquake Engineering and Soil Dynamics*, Vol.15, 1987, pp. 711-729.
- (13) Makris, N., D. Badoni, E. Delis, and G. Gazetas, "Prediction of Observed Bridge Response with Soil-Pile-Structure Interaction," *Journal of Structural Engineering*, ASCE, Vol. 120, No. 10, October 1982, pp. 2992-3011.
- (14) Zhang, J. and N. Makris, "Seismic Response Analysis of Highway Overcrossings Including Soil-structure Interaction," Pacific Earthquake Engineering Research Center, PEER 2001/02, March 2001.
- (15) *ACI-ASCE Committee 352, "Recommendations for design of beam-column joints in monolithic reinforced concrete structures," ACI Journal*, Vol. 82, No. 3, 1985, pp. 266-283.
- (16) American Concrete Institute Committee 318, "Building Code Requirements for Reinforced Concrete (ACI 318-99) and Commentary (ACI 318R-99)," Farmington Hills, Michigan, 1999.
- (17) Laplace, P., D.H. Sanders, M. Saiidi, and B. Douglas, "Shake Table Testing of Flexure Dominated Reinforced Concrete Bridge Columns," *Report No. CCEER-99-13*, Department of Civil Engineering, University of Nevada, Reno, December 1999.
- (18) Schmertmann, J. M., J.P. Hartman, and P.R. Brown, "Improved Strain Influence Factor Diagram," *ASCE Geotechnical Engineering Journal*, v104, 1978, pp. 1134.
- (19) El-Gamal, M., R. Siddharthan, and E.A. Maragakis, "Nonlinear Bridge Abutment Stiffnesses: Formulation Verification and Design Curves," *Rept. No. CCEER 95-01*, College of Engineering, University of Nevada, Reno, 1995, pp. 12-14.
- (20) Elton, D. J. "Settlement of Footings on Sand by CPT data," *Journal of Computing in Civil Engineering*, 1(2), April 1987, pp. 99-113.
- (21) Maugeri, M., F. Castelli, M.R. Massimino, and G. Verona, "Observed and Computed Settlements of Two Shallow Footings on Sand," *Journal of Geotechnical and Geoenvironmental Engineering*, 124(7), July 1998, pp 595-605.
- (22) Skiles, D. L., and F.C. Townsend, "Predicting Shallow Foundation Settlement in Sands from DMT," *Geotechnical Special Publication Proceedings of the Conference on Vertical and Horizontal Deformations of Foundations and Embankments. Part 1 of 2*, June 1994, 16-18, 1(40). Pub. ASCE, New York, NY, pp 132-142.

- (23) Ghionna, V. N., M. Manassero, and V. Peisino, "Settlements of Large Shallow Foundations on a partially cemented gravelly sand deposit using PLT data," *Proc Int Conf Soil Mechanics and Foundation Engr Deformation of Soils and Displacements of Structures*, May 1991 v 1, pp. 417-422.
- (24) Seed, H. B., and I.M. Idriss, "Soil Moduli and Damping in Soils, Design Equation and Curves." *Rep. No. EERC 70-10*, Earthquake Engineering Research Center, University of California, Berkeley, 1970.
- (25) Lindley, P. B., "Engineering Design with Natural Rubber," *NR Technical Bulletin*, The Malaysian Rubber Producers' Research Association, 1970, pp. 8-9.
- (26) Priestley, M., F. Seible, and M. Calvi, Seismic Design and Retrofit of Bridges, Wiley-Interscience, 1996.

Table 2.1 Measured Concrete Compressive Strength

As-Built Footing	Sample #1 ksi (MPa)	Sample #2 ksi (MPa)	Sample #3 ksi (MPa)	Average ksi (MPa)
7 Day	4.11 (28)	4.60 (31.4)		4.35 (29.7)
14 Day	4.42 (30.17)	4.96 (33.86)		4.69 (32)
28 Day	4.54 (31)	5.43 (37.07)		4.985 (34)
Day of Test	8.74 (60)	8.40 (57.34)		8.57 (58.5)
Column	Sample #1 ksi (MPa)	Sample #2 ksi (MPa)	Sample #3 ksi (MPa)	Average ksi (MPa)
7 Day	2.6 (17.75)	2.68 (18.30)	2.75 (18.77)	2.68 (18.30)
14 Day	3.32 (22.66)	3.41 (23.28)	3.6 (24.60)	3.44 (23.48)
28 Day	4.75 (32.43)	4.48 (30.58)	4.64 (31.68)	4.62 (31.54)
Day of Test	6.12 (41.78)	6.4 (43.7)	6.26 (42.74)	6.26 (42.74)
Beam	Sample #1 ksi (MPa)	Sample #2 ksi (MPa)	Sample #3 ksi (MPa)	Average ksi (MPa)
7 Day	3.36 (22.94)	3.05 (20.82)	3.51 (23.96)	3.31 (22.60)
14 Day	3.95 (30.00)	3.99 (27.41)	4.05 (27.64)	3.99 (27.24)
28 Day	4.11 (28.05)	3.85 (25.94)	4.09 (27.92)	4.02 (27.44)
Day of Test	5.29 (36.11)	5.17 (35.30)	5.41 (36.93)	5.29 (36.11)
Retrofitted Footing	Sample #1 ksi (MPa)	Sample #2 ksi (MPa)	Sample #3 ksi (MPa)	Average ksi (MPa)
7 Day	2.35 (16.04)	2.41 (16.45)	2.41 (16.45)	2.39 (16.31)
14 Day	3.34 (22.80)	3.22 (21.98)	3.37 (23.00)	3.31 (22.60)
28 Day	4.01 (27.37)	3.79 (25.87)	3.61 (24.64)	3.81 (26.01)
Day of Test	4.41 (30.11)	4.4 (30.04)	4.35 (29.70)	4.39 (29.97)

Table 2.2 Measured Tensile Strength of Steel Reinforcement

Bar Size	Yield Stress ksi (MPa)	Ultimate Strain	Ultimate Stress ksi (MPa)
#3 9.5 mm	66.33 (452.8)	0.183	110.66 (755)
#4 12.7 mm	63.33 (432.4)	0.165	104.33 (712.3)
#5 15.9 mm	65 (443.8)	0.192	110 (751)

Table 2.3 Testing Program for B2SA

Run Number	Motion	Peak Table Acceleration (g)
1	0.1 x Sylmar	0.06
2	0.2 x Sylmar	0.12
3	0.3 x Sylmar	0.18
4	0.4 x Sylmar	0.24
5	0.5 x Sylmar	0.30
6	0.6 x Sylmar	0.36

Table 2.4 Testing Program for B2SA

Run Number	Motion	Peak Table Acceleration (g)
1	0.1 x Sylmar	0.06
2	0.2 x Sylmar	0.12
3	0.3 x Sylmar	0.18
4	0.4 x Sylmar	0.24

Table 2.5 Testing Program for B2SF

Run Number	Motion	Peak Table Acceleration (g)
1	0.1 x Sylmar	0.06
2	0.2 x Sylmar	0.12
3	0.3 x Sylmar	0.18
4	0.4 x Sylmar	0.24
5	0.5 x Sylmar	0.30
6	0.6 x Sylmar	0.36
7	0.8 x Sylmar	0.48
8	1.0 x Sylmar	0.60
9	1.25 x Sylmar	0.75
10	1.50 x Sylmar	0.90
11	1.75 x Sylmar	1.05
12	1.90 x Sylmar	1.14
13	2.00 x Sylmar	1.20

TABLES

Table 3.1 Summary of Results for Soil Stiffnesses

	As-Built Model Footing	Retrofitted Model Footing	As-Built Prototype Footing	Retrofitted Prototype Footing
Dimensions B x L x T (m)	36"x32"x7" (0.92x0.82x0.18)	42"x48"x12" (1.07x1.22x0.3)	12'x10.7'x2.3' (3.67x3.25x0.72)	14'x16'x4' (4.3x4.9x1.22)
B', ft (m)	-	-	11.28 (3.46)	15 (4.6)
D, ft (m)	-	-	5 (1.53)	5 (1.53)
K _v , k/in (kN/mm)	849 (150.0)	1,904 (333.5)	3,396 (600.2)	7,616 (1,334)
K _h , k/in (kN/mm)	574 (100.5)	1,364 (238.8)	2,296 (402.0)	5,454 (955.0)
K _{v provided} , k/in (kN/mm)	657 (115.0)	1,163 (203.6)	-	-
K _{h provided} , k/in (kN/mm)	635 (111.2)	1,064 (186.3)	-	-

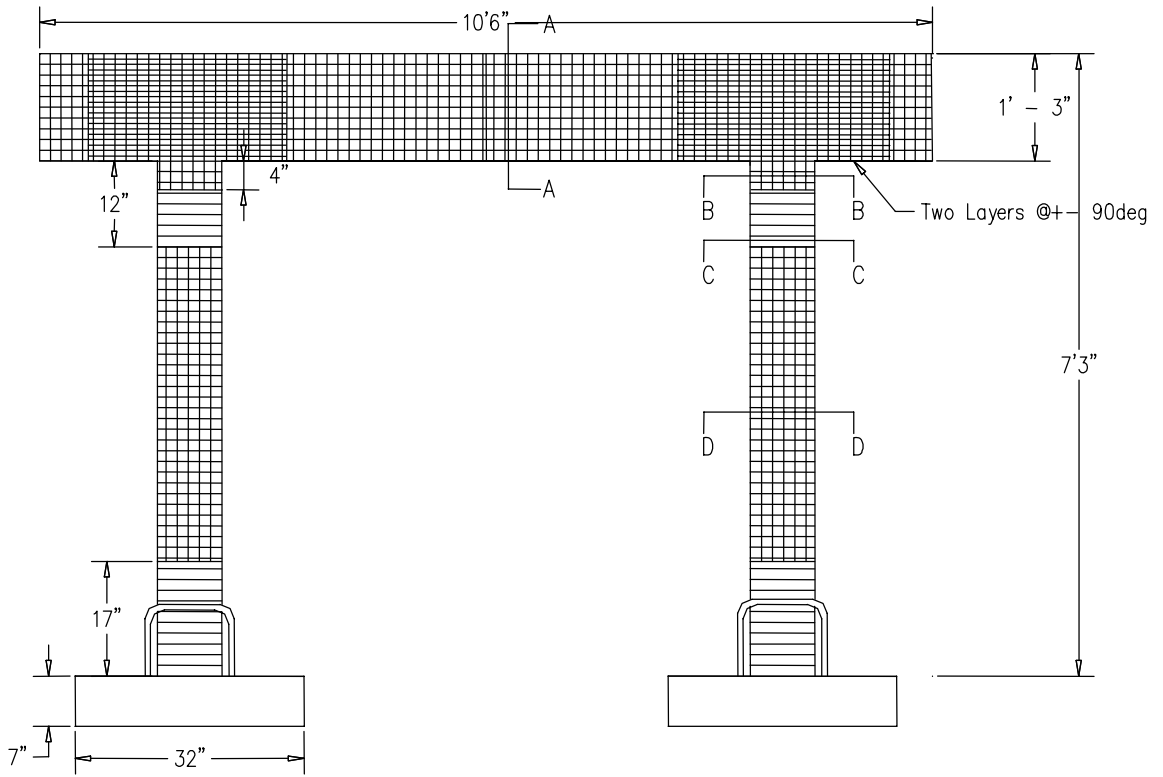


Fig. 2.1 Elevation of B2SA

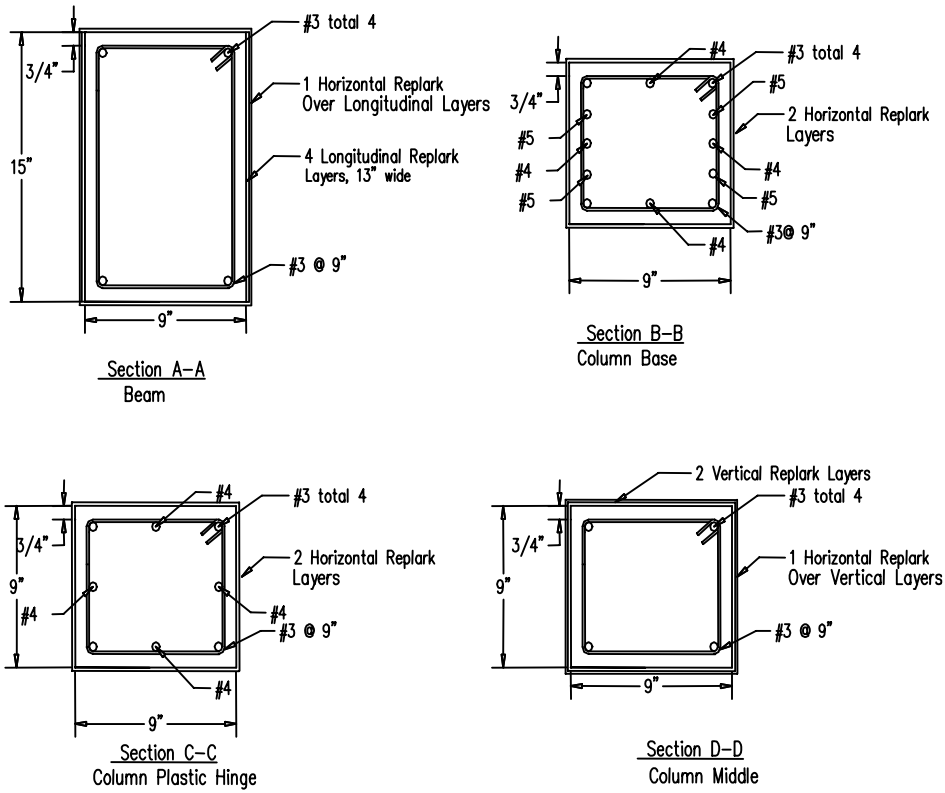


Fig. 2.2 Cross Sections for the Beam and Columns

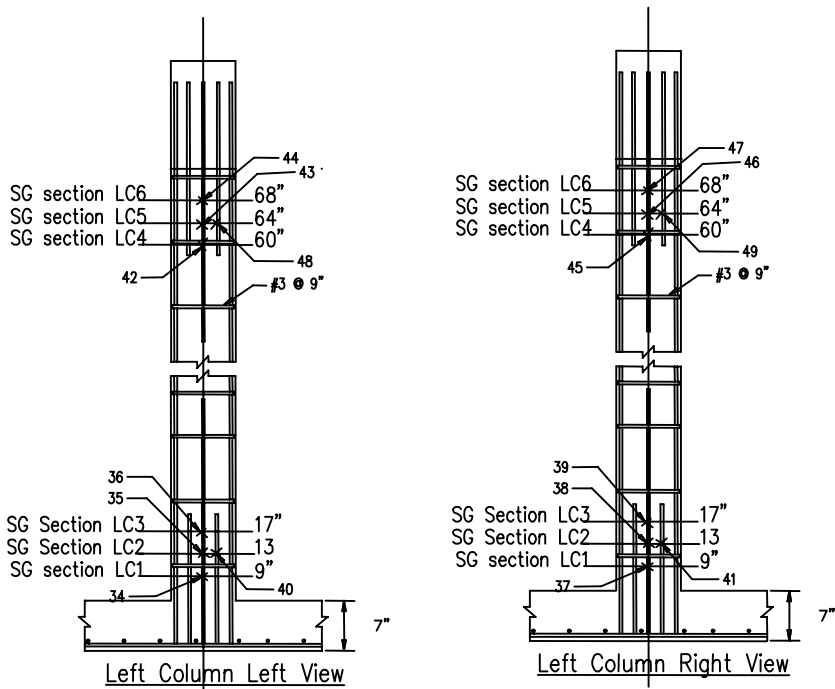


Fig. 2.3 Steel Details and Gage Locations for the Left Column in B2SA

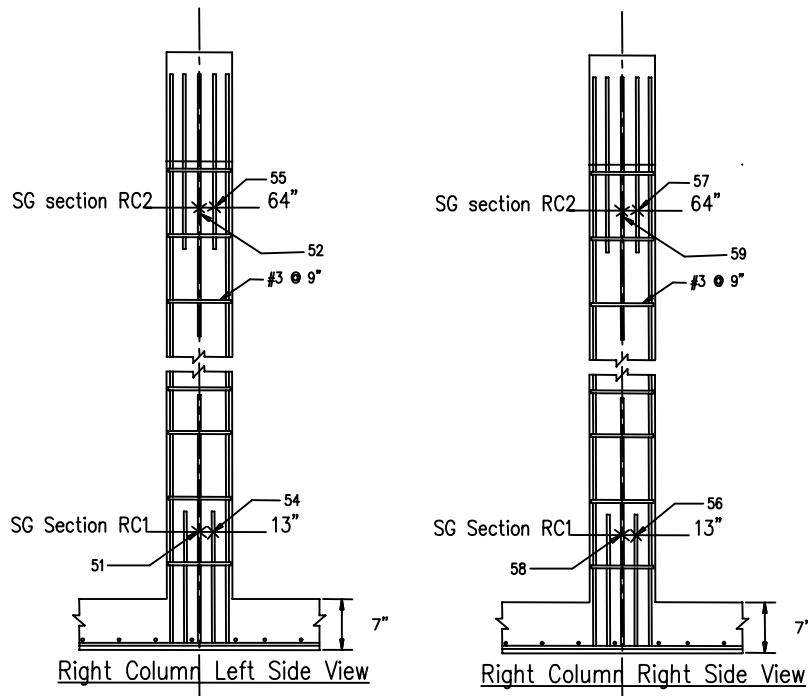


Fig. 2.4 Steel details and Gage Locations for the Right Column in B2SA

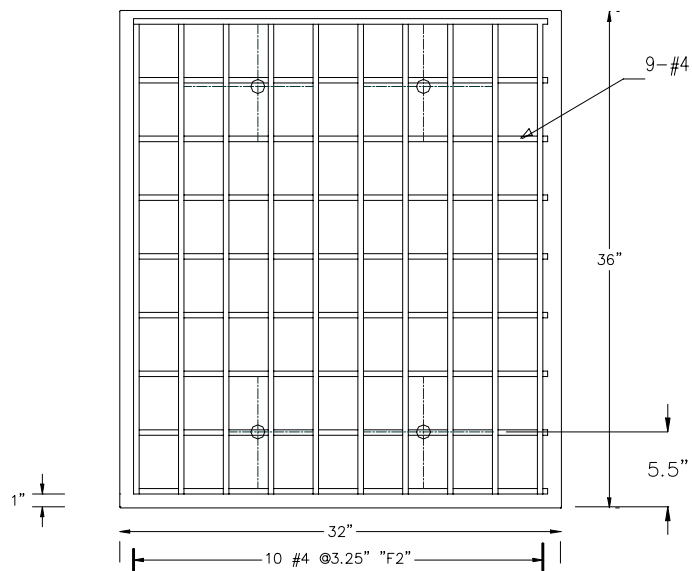


Fig. 2.5 Plan View of the As-built Footings

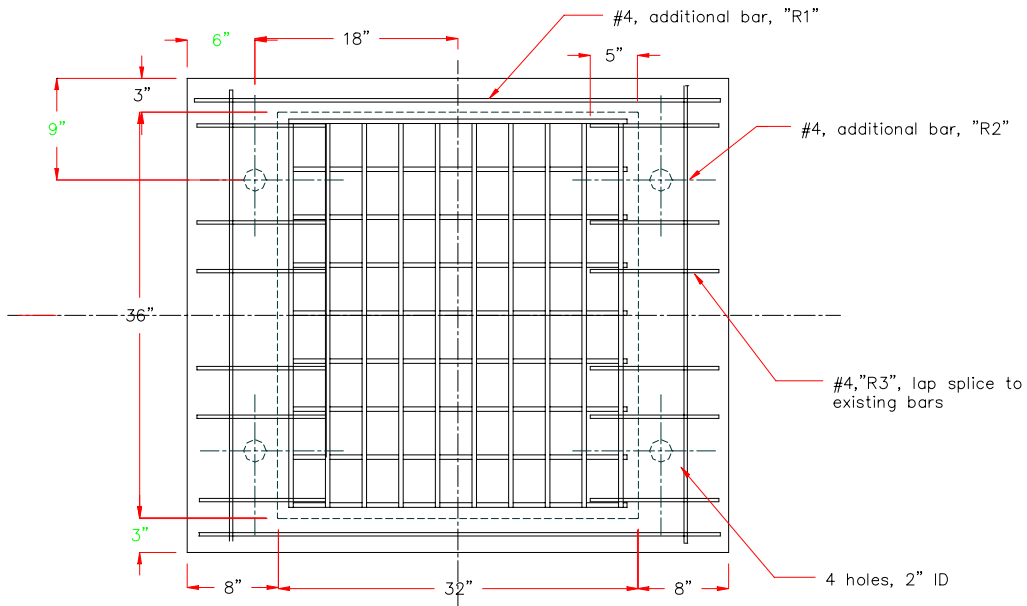


Fig. 2.6 Plan View of the Retrofitted Footings

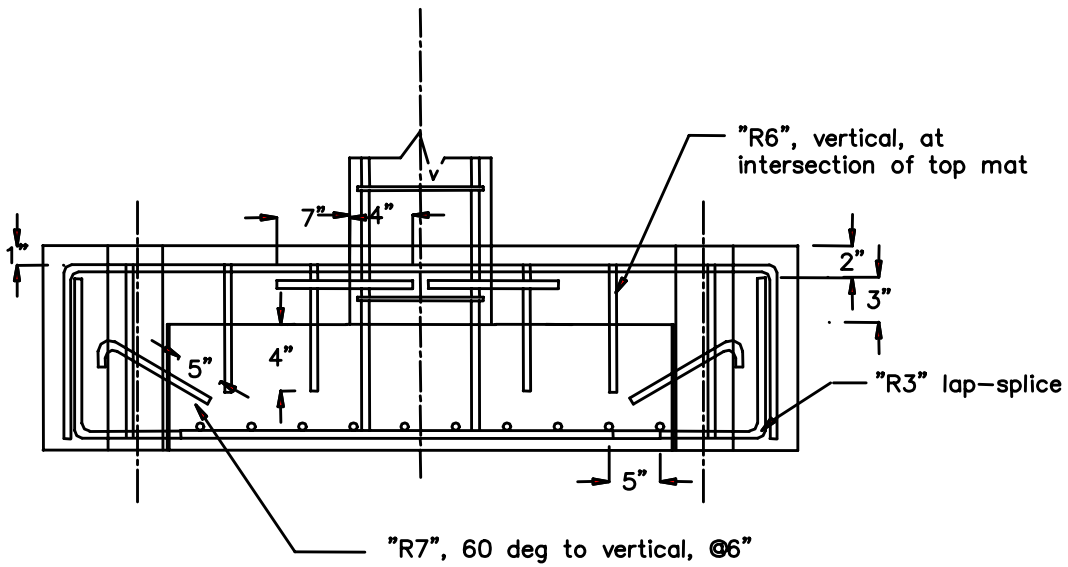


Fig. 2.7 Elevation View of the Retrofitted Footings

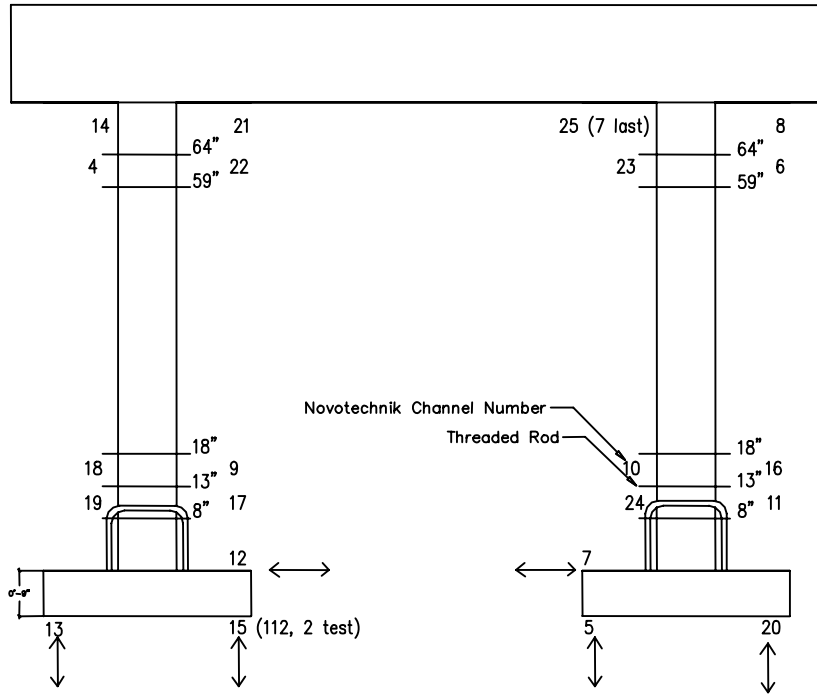


Fig. 2.8 Location of Threaded Rods for Curvature Measurement

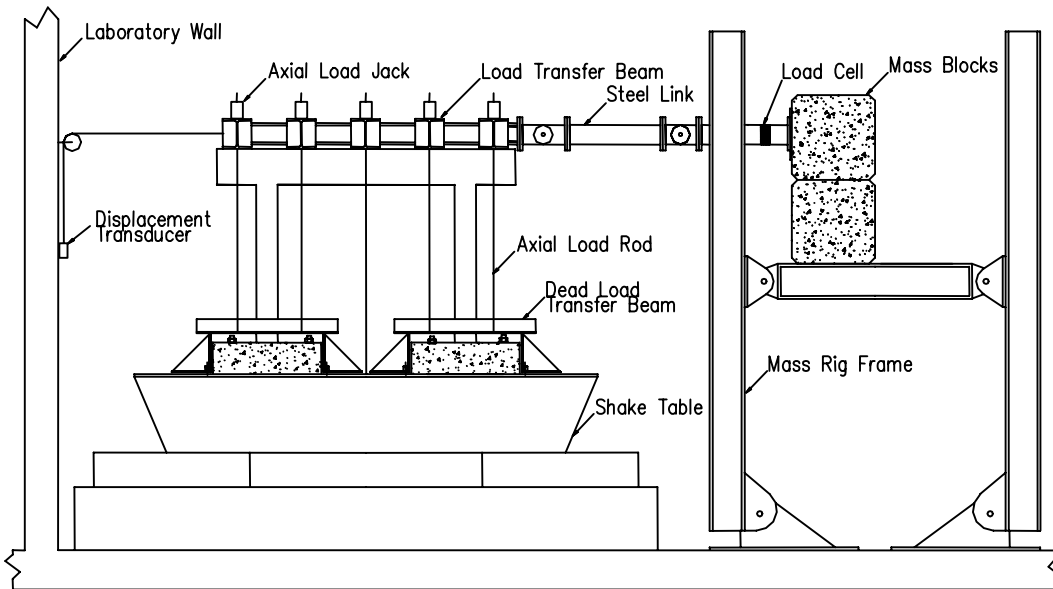


Fig. 2.9 Overall Test Set Up

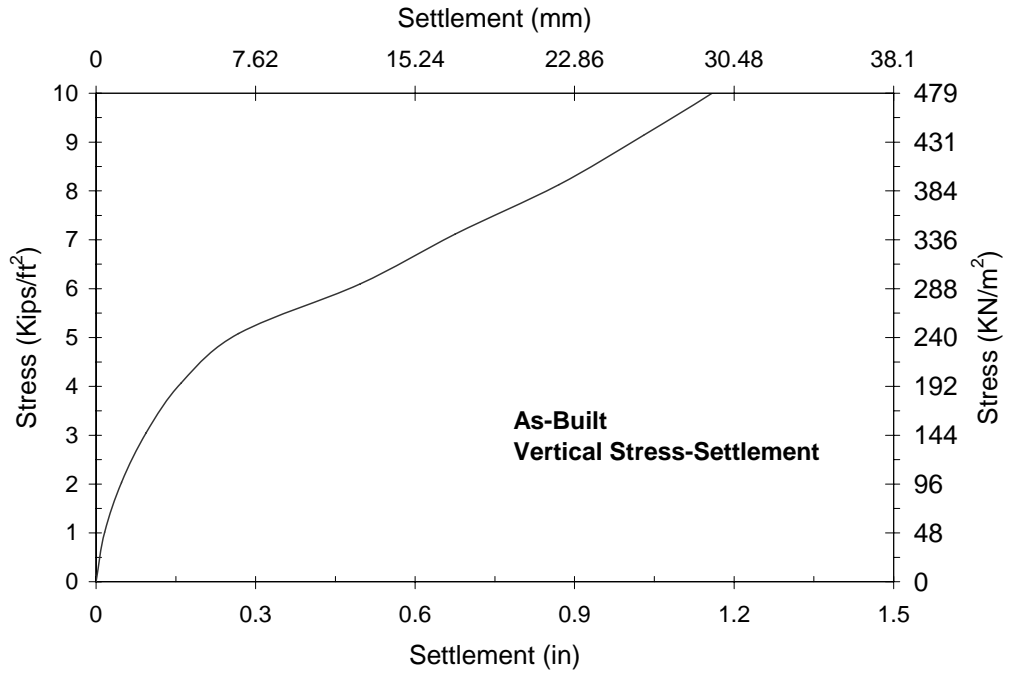


Fig. 3.1 Vertical Stress-settlement Relationship for the As-built Footing

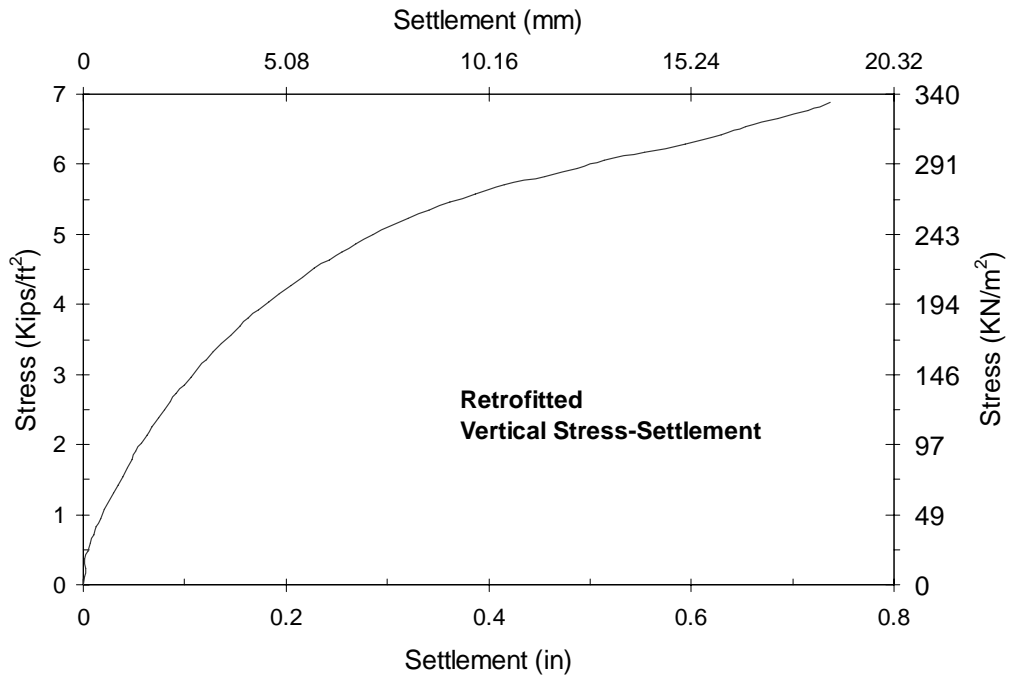


Figure 3.2 Vertical Stress-settlement Relationship for the Prototype Retrofitted Footing

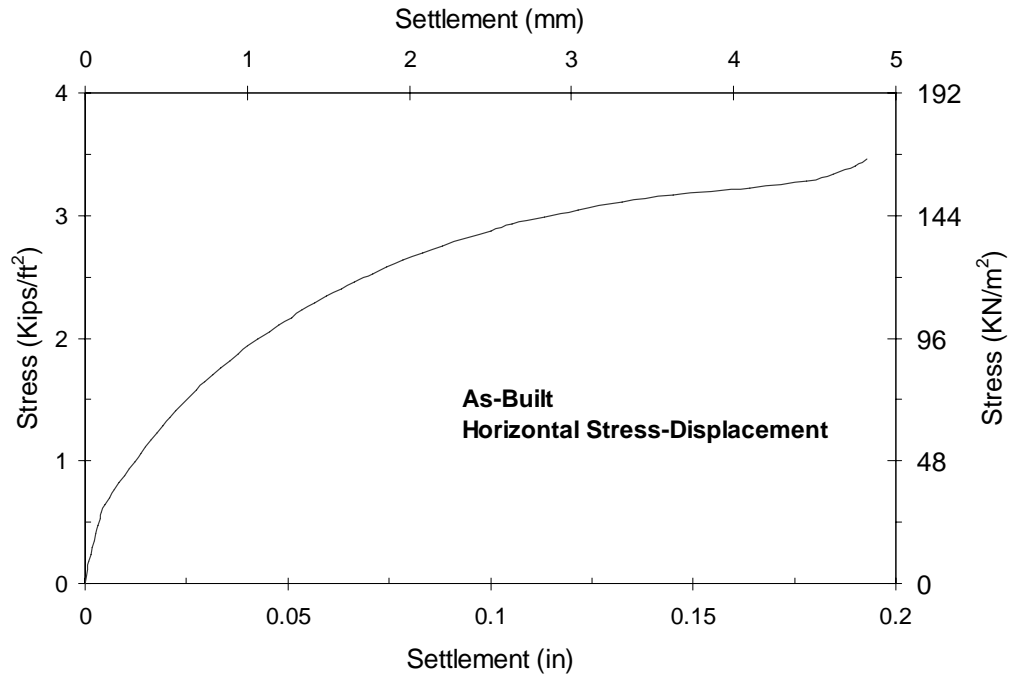


Fig. 3.3 Horizontal Stress-displacement for Prototype As-built Footing

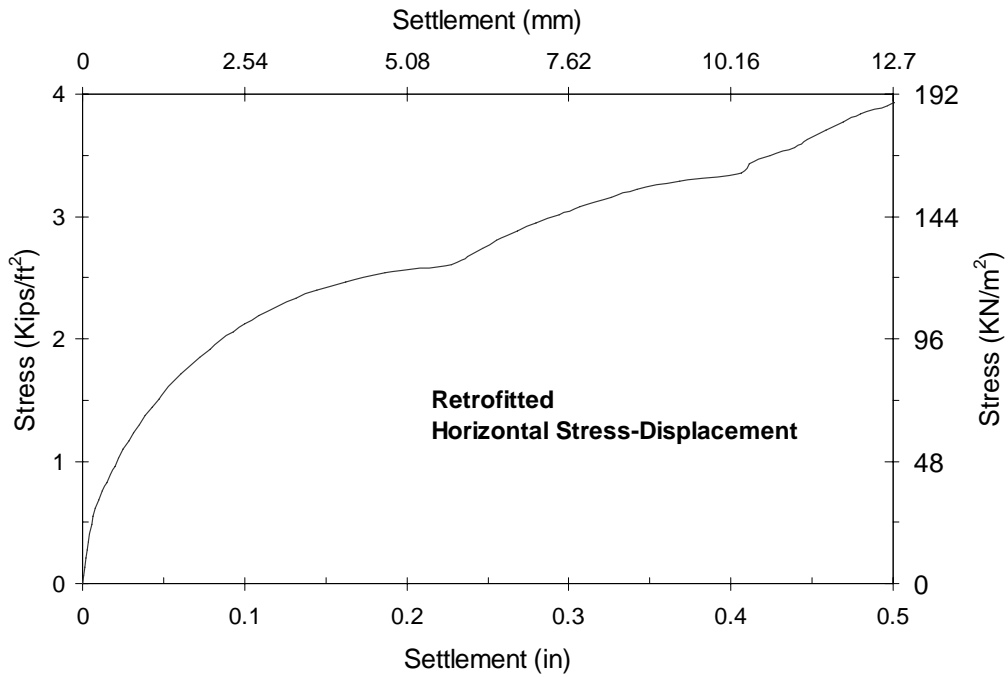


Fig. 3.4 Horizontal Stress-displacement for Retrofitted Prototype Footing

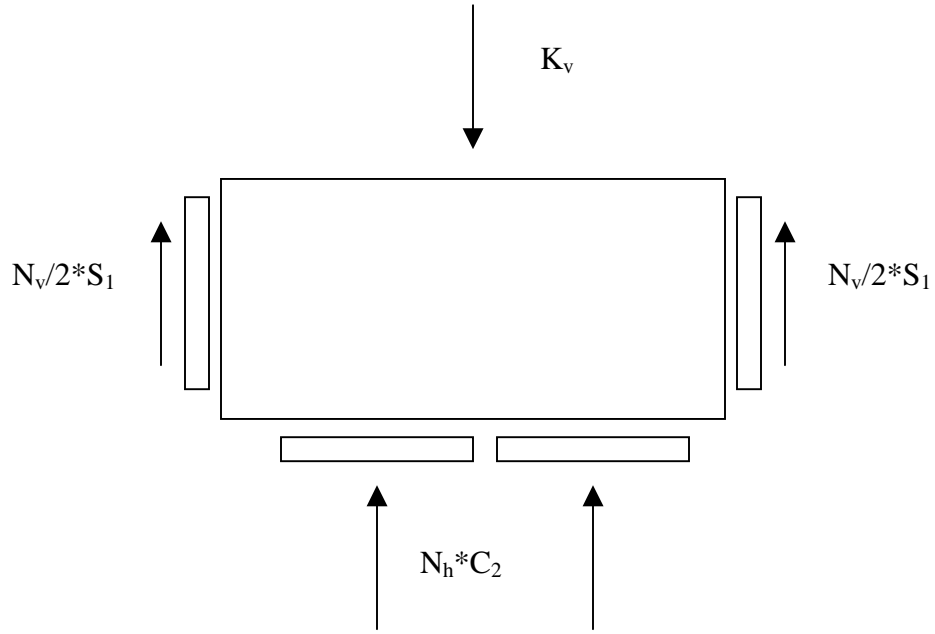


Fig. 3.5 Forces on Footing for Unit Downward Displacement

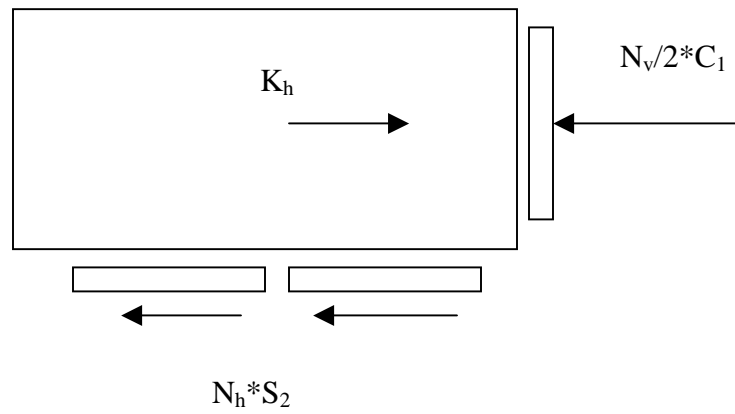


Fig. 3.6 Forces on Footing for Unit Horizontal Displacement



Fig. 3.7 Retrofitted Footing with Bearing Pads Highlighted for Clarity